JOURNAL OF COATING TECHNOLOGY AND INNOVATION
Apr-Jun 2024, VOL. 2, ISSUE 2, pp. 10-18
https://doi.org/10.61577/jcti.2024.100007

RESEAPRO JOURNALS

ORIGINAL ARTICLE

OPEN ACCESS

Al_2O_3-siloxane nanocomposite superhydrophobic coating on low carbon steel with improved corrosion resistance and stability upto 750°c by electrophoretic deposition

Laxmidhar Besra[1,2], Sanjukta Dey[1,2], Bimal P. Singh[1,2], Shubhra Bajpai[1,2], Bikash K. Jena[1,2], Tapan K. Rout[3] and Dilip K. Sengupta[3]

[1]CSIR-Institute of Minerals & Materials Technology, Bhubaneswar, Odisha, India
[2]Academy of Scientific and Innovative Research (AcSIR)[2], Rafi Marg, Anusandhan Bhavan, New Delhi, India
[3]Research and Development, Tata Steel Ltd., Jamshedpur, India

ABSTRACT

A durable nanocomposite film made of Al_2O_3 and siloxane, 30 µm thick with a water contact angle of 151°, was created on low carbon steel using electrophoretic deposition (EPD), then dip-coated in methyl hydrogen polysiloxane (KF-99) and cured at 140°C for 2 hours. The coating showed impressive resistance to corrosion, increasing the corrosion potential (E_{corr}) from -930 to -498 mV and decreasing the corrosion current (I_{corr}) from 120.22 to 1.122 µA/cm^2. Furthermore, there was a significant increase in the charge transfer resistance (Rct) from 10.84 to 8.7 x 10^6 Ω. These enhancements achieve an impressive 99.1% efficiency in inhibiting corrosion. The coating showed stability up to 750°C, while achieving a corrosion inhibition efficiency of 98.3%.

KEYWORDS

Al_2O_3-siloxane nanocomposite coating; Low carbon steel; Electrophoretic deposition; Superhydrophobic; Corrosion resistance; High temperature stability

ARTICLE HISTORY

Received 13 January 2024;
Revised 07 February 2024;
Accepted 27 March 2024

Introduction

The corrosion of metals and metal alloys is a major worldwide problem that affects different engineering systems like pipelines, cars, and planes. Rusting is the most common type of corrosion, especially in metals such as iron and steel. Rusting occurs naturally as a thermodynamically favorable process, causing metals/alloys to change from higher energy states (finished products) to lower energy states (ores and rust). The worldwide expense from corrosion surpasses $2.5 trillion per year, with India facing expenses around $26.1 billion annually [1,2]. Utilizing more advanced methods to prevent corrosion could result in savings of 15-35% of these expenses [2]. Common methods for reducing damage include protective coatings, anodic or cathodic protection, corrosion inhibitors, and alloy and composite coatings [3-10]. Although they work well, there is an increasing need for stronger technologies that can function efficiently in extremely harsh conditions, in order to prolong the lifespan of metals and reap environmental and economic advantages.

Corrosion of mild steel is especially severe in high salinity seawater with micro-organisms present [10]. In order to effectively address corrosion, new methods are required due to the scale and expense of the issue. Superhydrophobic surfaces are receiving notable interest for reducing corrosion because of their outstanding ability to repel water [11,12]. Water repellency levels are determined by hydrophobicity and contact angle; surfaces with a water contact angle above 150° are considered superhydrophobic. Controlling the chemical composition (low surface energy) and surface roughness can be used to create these surfaces [12-14]. Different methods have been documented for creating superhydrophobic surfaces on materials such as steel, copper, and aluminum in order to enhance their ability to resist corrosion [12,14,15]. Nevertheless, developing artificial superhydrophobic surfaces that imitate lotus leaves with straightforward fabrication methods suitable for industrial use is still a major obstacle [16].

Electrophoretic deposition (EPD) is a well-known industrial technique employed in a range of applications [17-19]. Applying materials of various sizes, from sub-microns to nanometers, onto conductive surfaces is efficiently done. EPD is adaptable, speedy, and economical, providing effective management of stoichiometry, microstructure, and properties [18-20]. Recently, there have been new developments in EPD, such as the creation of superhydrophobic coatings. There is a growing interest in employing EPD for producing superhydrophobic coatings on metals to prevent oxidation and corrosion.

Recent studies have shown the possibilities of using superhydrophobicity to prevent corrosion. According to Zhang-Fang et al., superhydrophobic films have the potential to be used instead of chromate-based coatings for metal protection, with findings showing that these films can greatly improve the corrosion resistance of metals [21]. In their study, Mohamed et al. thoroughly examined how superhydrophobic surfaces behave in corrosion situations and explored their use in protecting against corrosion [11]. Ishizaki and colleagues created a highly water-repellent surface on magnesium alloy by applying trimethyl-methoxysilane molecules. They used electrochemical impedance spectroscopy to analyse its ability to resist corrosion in a NaCl water solution [12]. Sanjukta and her team recently published a study on the effectiveness of superhydrophobic coatings on mild steel that were treated with titanium oxide and methylhydrogen polysiloxane when exposed to a 3.5 wt% aqueous NaCl solution in terms of preventing corrosion [22].

*Correspondence: Dr. Laxmidhar Besra, Department of Material Chemistry, CSIR-Institute of Minerals & Materials Technology, Bhubaneshwar, India, 751013, Tel/ Fax: +91 674 2379244, e-mail: ldbesra@immt.res.in

Low carbon steel is commonly utilized in various industries including automotive, construction, and cookware due to its favorable mechanical characteristics and the ease with which welds can be achieved. Nevertheless, its high vulnerability to corrosion when exposed to water restricts its widespread utilization in new developments. Preventing steel from coming into contact with aqueous environments is essential in order to inhibit corrosion. Hence, superhydrophobic coatings show great potential in enhancing corrosion resistance by blocking direct contact between water and the steel surface.

The main goal of this research is to establish a method for applying a surface coating on low carbon steel in order to stop moisture from penetrating. This research describes an inexpensive and straightforward method for creating superhydrophobic surfaces and assessing how well they resist corrosion on mild steel. It involves applying a colloidal alumina suspension, then heat-treating a dip-coated KF-99 film made from methylhydrogen polysiloxane grown through EPD at ambient temperature. The decision to use aluminum oxide (Al_2O_3) as the coating material was based on its extremely high hardness and stability in electrochemical reactions, ensuring the surface is both mechanically strong and resistant to corrosion. Analysis of the coating's structure was carried out through the use of scanning electron microscopy (SEM) and field emission scanning electron microscopy (FESEM). Surface profiler was used to measure the roughness of the surface. The samples were evaluated for their corrosion resistance and wettability using electrochemical and contact angle tests. Moreover, a microscratch adhesion test was conducted to assess the adhesion of the coating to the surface.

This method seeks to meet the pressing demand for efficient ways to prevent corrosion by utilizing the advantages of superhydrophobic surfaces to improve the strength and lifespan of low carbon steel in different uses.

Experiment

Materials

A steel base with low carbon content (0.2% C, 1.5% Mn, 0.5% Si, 0.02% P, 0.5% Cr, 0.04% Ti, 0.005% B, and 97.2% Fe) measuring 5 cm x 2 cm x 1 mm was used. Alumina powder with an average particle size of 250 nm (AKP-50, Sumitomo Corporation, Chuo-Ku, Tokyo, Japan) was utilized. The coupling agent used to increase hydrophobic properties was Methylhydrogen polysiloxane (KF-99, Shin-Etsu Chemical, Tokyo, Japan). Dispersants and pH control agents were introduced into the system with the use of Polyethylene imines (PEI) and Phenyl-phosphonic acid (Sigma-Aldrich, USA) respectively. The combination of these materials is intended to enhance the performance of the substrate using advanced surface treatment methods, thus promoting innovation in material engineering. [13,14]. These composites leverage the synergy between graphene and other materials to enhance photocatalytic efficiency, aiding in the breakdown of environmental pollutants.

Substrate preparation

Thorough substrate cleaning is essential for top-notch coatings. The steel samples were first cleaned by soaking in a 5 wt% HF solution for 5 seconds, then subjected to ultrasonication in ethanol and acetone for 10 minutes each. After cleaning, the surfaces were coated with an aluminum phosphate monobasic solution (Sigma Aldrich, USA) to prevent oxidation and improve surface roughness. In this phosphating process, the cleaned steel substrates are immersed in a heated aluminum phosphate monobasic solution (50°C) for 10 minutes, then washed thoroughly with water to eliminate excess phosphating residues. The materials were subsequently dried in the open air at ambient conditions.

Preparation of composite coating

Electrophoretic Deposition (EPD) was used to produce a corrosion-resistant coating with superhydrophobic properties. The EPD arrangement consisted of two low-carbon steel plates placed parallel with a 1 cm gap between them. The phosphate steel plate was used as the cathode, and the cleaned steel plate was utilized as the anode. The deposition was carried out using a DC source meter (Model 2410, Keithley Instruments, Inc, USA) in constant voltage mode. Applying a voltage of 100V for 30 seconds led to a consistent 30µm thick deposit. After depositing the green coating, great care was taken to remove the substrate without disturbing the new coating. After that, the samples were dip-coated with KF-99 for a duration of 10 minutes and subsequently underwent annealing at 140°C for a period of 2 hours in order to finish the coating procedure. Figure 1 illustrates a schematic summary of the manufacturing procedure. This technique guarantees a consistent, long-lasting layer that improves the substrate's ability to resist corrosion while maintaining its superhydrophobic properties.

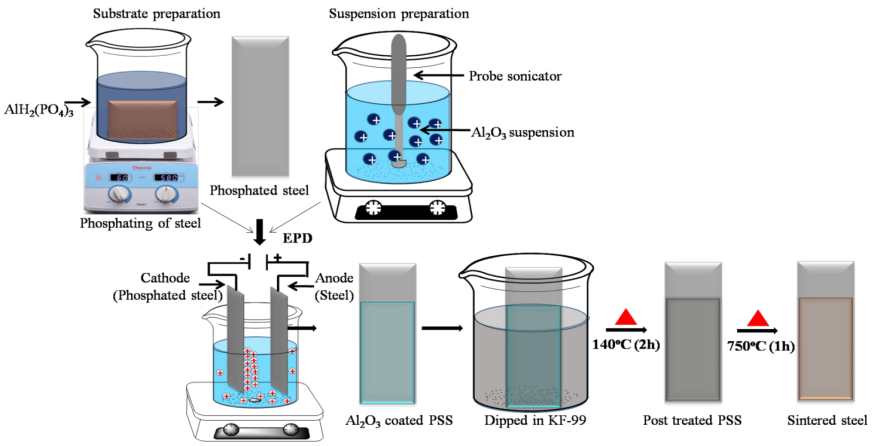

Figure 1. Schematic representation for fabrication of superhydrophobic coating as a corrosion barrier by EPD technique.

https://doi.org/10.61577/jcti.2024.100007

Characterization

The contact angle meter (Data Physics, OCA-15EC, Filderstadt, Germany) was used to measure the static water contact angle (WCA) at five different points on the surface of both coated and uncoated samples at room temperature (25°C). The findings presented in this document represent the mean of these five observations. The field emission scanning electron microscope (FESEM) (SUPRA 55, Zeiss Instrument, Germany) and scanning electron microscope (SEM) (Hitachi, S-3400N, Tokyo, Japan) were used to observe the coating morphologies. The roughness of the coating was evaluated with a stylus profiler (Nano Map, AEP Technology, New York, USA). FTIR spectra of coatings were obtained using a Perkin Elmer Spectrum Gx instrument based in Norwalk, CT, USA for chemical analysis. The adhesion properties of the coating were assessed by utilizing the micro scratch adhesion tester (UMT, Bruker CETR) with a Rockwell-C spherical indenter of 200µm diameter.

Electrochemical properties and stability of suspension

The standard three-electrode setup on a Chi 660D electrochemical workstation (Austin, U.S.A.) was used for the electrochemical studies. In this setup, a platinum wire was the counter electrode, an Ag/AgCl electrode served as the reference, and the working electrode was the Al_2O_3-coated sample. The working electrode was encased in epoxy resin to form a 1 cm × 1 cm surface. Samples were placed in a 3.5 wt% NaCl solution for 3 hours before taking measurements to stabilize the potential. The OCP was measured for 1 hour prior to performing PPC and EIS. PPC involved scanning a potential range of -1.5V to 0.5V at a rate of 1 mV/s to determine corrosion potential (E_{corr}) and corrosion current density (I_{corr}) through the extrapolation method. EIS tests were conducted at OCP, covering frequencies from 100 kHz to 1 mHz using a 10mV amplitude.

Results and Discussion

Particle size and Electrokinetics of Al_2O_3 suspension

In Figure 2, there is a TEM image of Al_2O_3, and the inset displays a selected area diffraction (SAED) pattern, which suggests that the Al_2O_3 powder is crystalline. The mean particle size was around 250 nanometers. The alumina suspension had a pH of approximately 6.7 in ethanol, resulting in a positive surface charge of +180 mV due to Al_2O_3 oxide removing H^+ ions. The reaction representing this protonation process is: $[M\text{-}O\text{-}H] + H^+ \leftrightarrow [M\text{-}O\text{-}H\text{-}H]^+$. Figure 3 depicts how the streaming potential of the Al_2O_3 suspension changes with pH. The preparation of a well-dispersed alumina suspension (1.5 wt%) involved dispersing the powder in 100 ml of ethanol using PEI as a dispersant, and then adjusting the pH to 3.8 with phenyl phosphonic acid. Sonication for 1 hour was conducted to maintain stability.

The SEM images in Figure 4 compare steel in its original state to steel that has been treated with phosphate. Phosphating was carried out to avoid the steel substrate from oxidizing and rusting after cleaning and during tests. This procedure resulted in the creation of a firmly attached layer of iron phosphate ($FePO_4$) on the surface of the steel, following the reaction:

$$Fe + Al(H_2PO_4)_3 \rightarrow FePO_4 + Al(OH)_3 + H \quad (1)$$

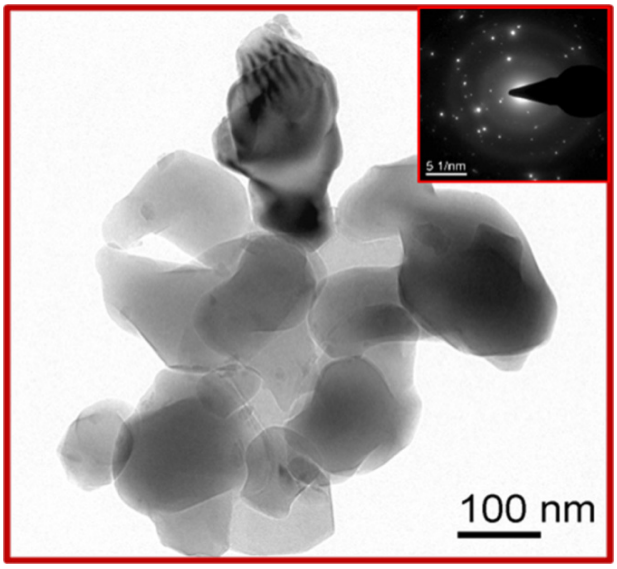

Figure 2. TEM of Al_2O_3 powder and inset: selected area diffraction pattern.

This shows how phosphating can improve the corrosion resistance of steel, while studying Al_2O_3 suspensions gives us information on their stability and surface charge.

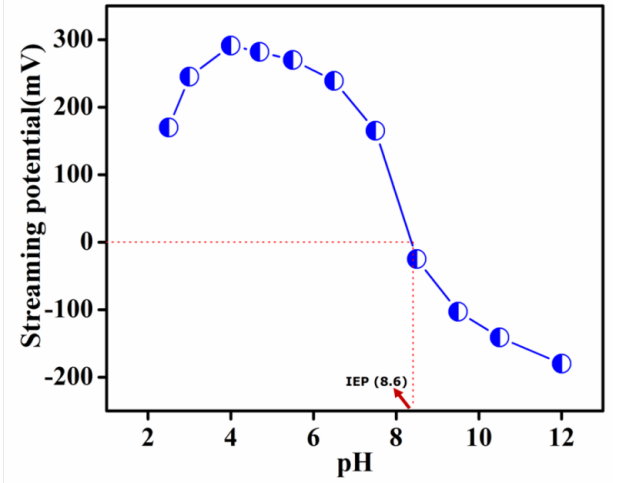

Figure 3. Streaming potential plot for Al_2O_3 suspension at different pH.

The SEM image (Figure 4b) clearly shows that the surface of PSS was rougher than that of bare steel. The bumpy texture of the inactive iron phosphate ($FePO_4$) on the steel is anticipated to not only stop oxidation from happening on its own, but also help improve the bonding of the coating [23].

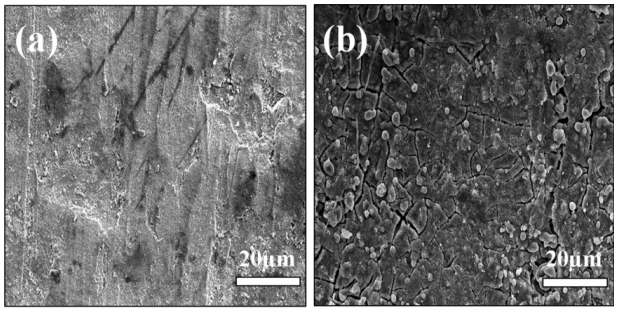

Figure 4. SEM images of (a) bare steel, and (b) phosphated steel.

https://doi.org/10.61577/jcti.2024.100007

Coating microstructure

Figure 5a displays FESEM pictures of PSS coated with Al_2O_3, showing a very porous microstructure. After treating with higher amounts of KF-99 (10-100 wt%) and then baking at 140°C for 2 hours (Figures 5(b-e)), the pores decrease significantly, resulting in a consistent, seamless, and crack-free layer. The sample coated with 100 wt% KF-99 shows a densely packed and compact coating, which is remarkable. Prior research has shown that in the presence of ethyl alcohol, KF-99 undergoes hydrolysis to mainly produce silanol and silane species [22]. These species form Al-O-Si and Fe-O-Si bonds by interacting with both the exposed metal surface and the coating surface [24].

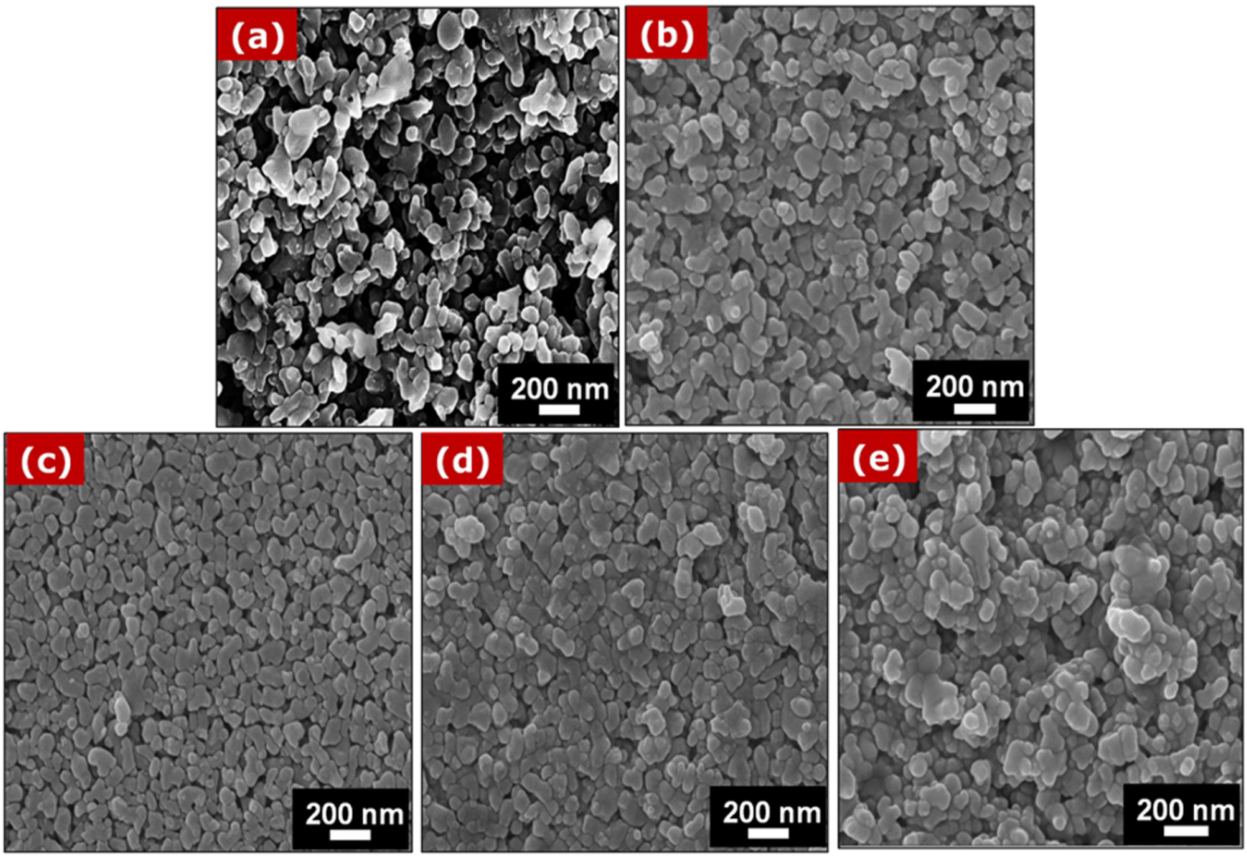

Figure 5. FESEM images of Al_2O_3 coated PSS (a), Al_2O_3 coated PSS post treated with 10 wt% (b), 20 wt% (c), 50 wt% (d), 100 wt% (e) KF-99, cured at 140°C for 2h.

Coating adhesion

Coatings' adhesive strength and crack propagation resistance were evaluated with a laboratory microscratch tester (UMT, Bruker CETR, USA) featuring a Rockwell-C spherical indenter (200 µm diameter). Experimental examinations were carried out using a method that included two steps: initially, a stable force of 5N was exerted for 10 seconds, then gradually increasing from 5 to 50N within 25 seconds at a speed of 5mm/min, leading to a scratch distance of 2mm in total. LC1 and LC2 were key parameters that were measured, with LC1 representing the load at crack initiation in the coating and LC2 representing the load at complete delamination between coating and substrate.

The formula CPR = $LC_1 \times (LC_2\text{-}LC_1)$ was utilized to determine the crack propagation resistance (CPR), giving information about the coating's resistance to crack propagation. At the same time, the friction coefficient (COF) was measured during the scan, and the COF value at LC2 showed the strength of adhesion in Table 1. A weaker adhesion is associated with a higher COF.

$$CPR = LC_1 (LC_2\text{-} LC_1) \quad (2)$$

Figure 6 shows the scratch test outcomes of alumina-coated PSS treated with different levels of KF-99 (10 wt%, 20 wt%, 50 wt%, and 100 wt%). Uncoated PSS without treatment showed weak adhesion (LC_1 = 5.5N) and low cohesive strength (16.5N). On the other hand, mechanical properties were significantly improved after treatment with KF-99. More precisely, the cohesion and toughness of the coating significantly improved as the CPR value rose from 16.64N with 10 wt% KF-99 to 159.3N with 100 wt% KF-99.

The untreated alumina-coated PSS showed a COF of 0.3, which reduced to 0.04 after treatment with 10 wt% KF-99, indicating enhanced adhesion. The most favorable adhesion, as shown by the lowest COF values, was found with a 10-20 wt% KF-99 treatment. Outside of this range, COF values experienced a slight increase but continued to stay relatively constant at approximately 0.15.

https://doi.org/10.61577/jcti.2024.100007

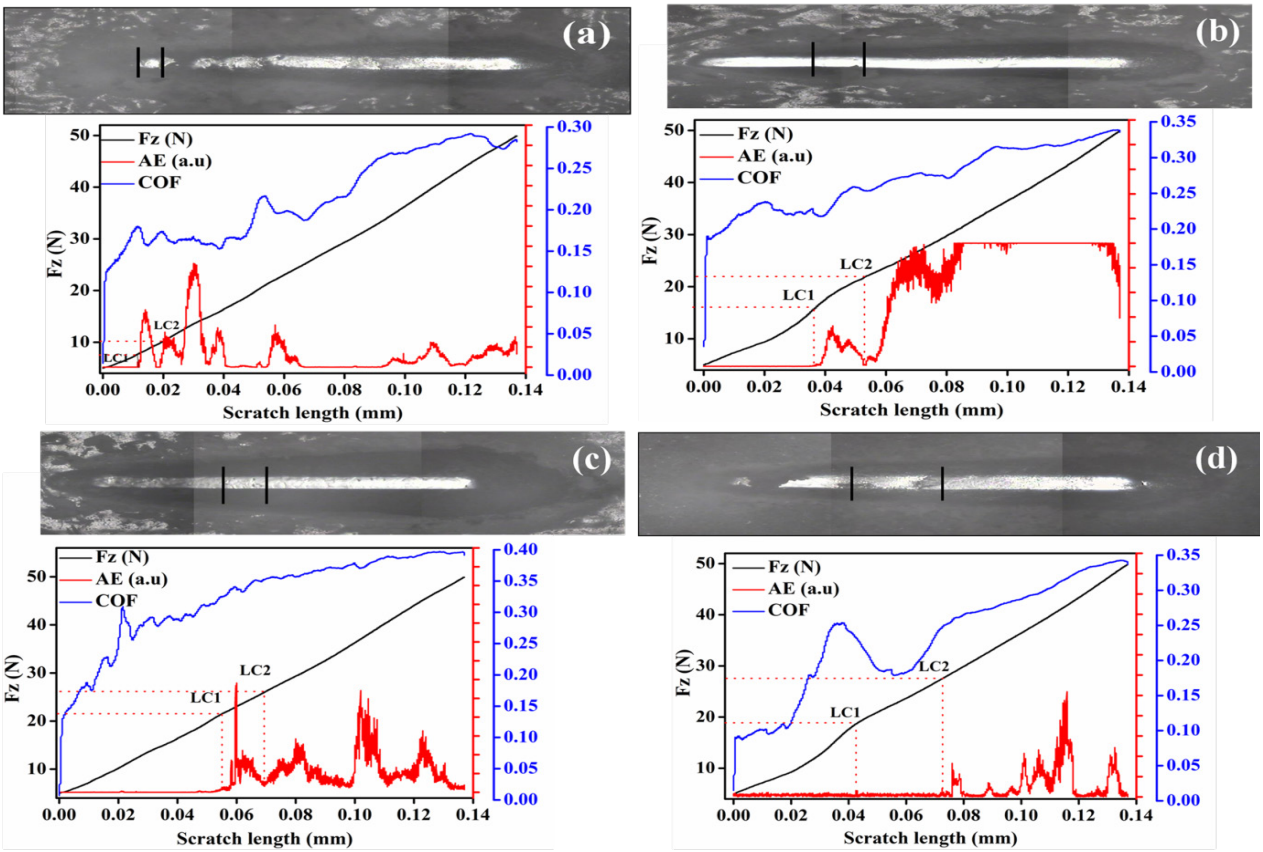

Figure 6. Scratch test results of Al_2O_3 coated PSS post treated with 10 wt% (a), 20 wt% (b), 50 wt% (c), 100 wt% (d) KF-99, cured at 140°C for 2h.

Table 1. Critical cracking load (LC1), Coating delamination load (LC2), Crack propagation resistance (CPR) and co-efficient of friction obtained from Figure 6.

Sample	LC_1 (N)	LC_2 (N)	CPR	COF
Alumina coated PSS	5.5	8.5	16.5	0.3
10 wt% KF-99	8.07	10.06	16.64	0.04
20 wt% KF-99	16.85	21.63	80.54	0.15
50 wt% KF-99	21.66	26.02	95.03	0.19
100 wt% KF-99	19.1	27.44	159.3	0.17

These results emphasize the important function of KF-99 treatment in improving the mechanical properties of alumina-coated PSS, demonstrating its potential in situations where strong adhesion and crack resistance are needed.

Electrochemical assessment and corrosion resistance of coatings

Figures 7 and 8 show important electrochemical assessments, specifically Tafel and Nyquist plots, that are utilized to evaluate the corrosion protection of different coatings. Figure 7 shows Tafel curves for various samples: untreated steel (a), PSS coated with Al_2O_3 (b), and Al_2O_3-coated PSS treated with different doses of KF-99 (c-f). Significantly, all plated samples exhibit a noteworthy increase in corrosion potential in comparison to uncoated steel (-930 mV). More precisely, the corrosion potentials of Al_2O_3-coated PSS and KF-99-treated specimens are: (b) -870 mV, (c) -515 mV, (d) -498 mV, (e) -580 mV, and (f) -570 mV. This change indicates improved ability to resist corrosion, which aligns with results from EIS analysis displayed in Figure 8.

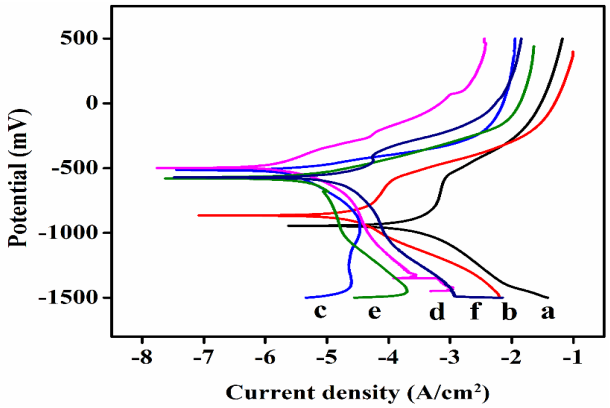

Figure 7. Tafel plots for steel (a), Al_2O_3 coated PSS (b), Al_2O_3 coated PSS post treated with 10 wt% (c), 20 wt% (d), 50 wt% (e), 100 wt% (f) KF-99, cured at 140°C for 2h.

Figure 8 shows Nyquist plots plotting the real part and the imaginary part of impedance. A complete semicircle on bare steel reveals a high susceptibility to corrosion. On the other

https://doi.org/10.61577/jcti.2024.100007

hand, coatings show flattened semicircles, indicating improved ability to resist charge transfer in corrosion processes. The resistance to corrosion (Rct) is determined by the radius of the semicircle and is inversely related to the corrosion rate. The Rct values measured on coated surfaces are significantly greater compared to those on untreated steel, strengthening the resistance to corrosion.

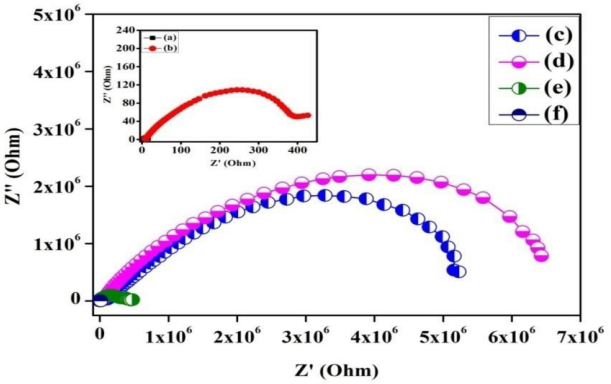

Figure 8. Nyquist plots for steel (a), Al_2O_3 coated PSS (b), Al_2O_3 coated PSS post treated with 10 wt% (c), 20 wt% (d), 50 wt% (e), 100 wt% (f) KF-99, cured at 140°C for 2h.

Corrosion parameters like corrosion potential (E_{corr}) and corrosion current density (I_{corr}) were determined from Tafel plots using Equation 3, where K1 is a constant, EW is equivalent weight, Icorr is corrosion current, and ρ represents density. The values were utilized for calculating corrosion rates, presented in Table 2. Equation 4 was used to calculate the inhibition efficiency (% η) of coatings with and without KF-99. For example, the PSS coated with 20 wt% KF-99 showed an efficiency of 99.1% after being baked at 140°C. Even after sintering at 750°C, the efficiency stayed high at 98.3%, demonstrating the longevity of the protective coating [25].

$$\text{Corrosion rate} = K1 \times EW \times Icorr/\rho \quad (3)$$

$$\eta = [I_{\text{bare steel substrate}} - I_{\text{20wt \% KF-99 coated substrate}}]/I_{\text{bare steel substrate}} \times 100 \quad (4)$$

In summary, the combination of Tafel and Nyquist analyses highlights the superior corrosion resistance of Al_2O_3-coated PSS and KF-99 treatments over untreated steel. These results are essential for applications that need strong protection against corrosion, providing an understanding of how engineered coatings perform and last in different environmental situations.

Table 2. E_{corr}, i_{corr}, values obtained from Figure 7, calculated corrosion rate, charge transfer resistance (Rct) values as obtained from Fig.8 for Al_2O_3 coated PSS post treated with varying dosages of KF-99.

Sample	E_{corr} (mV)	I_{corr} (μA/cm²)	Corrosion rate(mm/yr)	Inhibition Efficiency	Rct (Ω)
Cured at 140°C					
Bare steel	-930	120.22	1.2		10.84
Al_2O_3 coated PSS	-870	15.48	0.15	87.5	453.4
10 wt% KF-99	-515	1.91	0.02	98.3	5.7×10^6
20 wt% KF-99	-498	1.1	0.01	99.1	8.7×10^6
50 wt% KF-99	-580	1.34	0.01	99.1	6.4×10^5
100 wt% KF-99	-570	2.43	0.03	97.5	1.6×10^4
Sintered at 750 °C					
Bare steel	-930	120.22	1.2	-	-
20 wt% KF-99	-870	1.9	0.02	98.3	-

Wettability characteristics of coatings

Surface wetness is an important characteristic in coatings that significantly impacts their real-world uses, particularly in corrosion prevention [26]. Hydrophobic and superhydrophobic coatings are highly fascinating for their ability to resist corrosive liquids on metal surfaces [11]. Data on water contact angle and surface roughness of PSS coated with Al_2O_3 treated with different concentrations of KF-99 is shown in Figure 9. At first, the steel base showed very high water-attracting properties (11°), whereas the Al_2O_3-coated PSS without KF-99 treatment was water-loving (42.4°). Yet, treating with KF-99 at 10%, 20%, 50%, and 100% concentrations resulted in all coatings becoming hydrophobic with a contact angle exceeding 90°. More precisely, the contact angles for samples treated with 10%, 20%, 50%, and 100% KF-99 were found to be 148.3°, 151.2°, 142.5°, and 108.5°, respectively. The application of 10% KF-99 resulted in a nearly superhydrophobic coating (148.3°), whereas using 20% KF-99 led to superhydrophobic properties (contact angle > 150°).

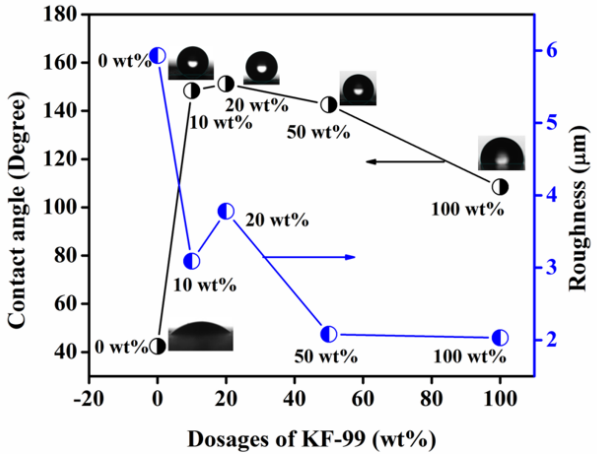

Figure 9. Surface contact angle and roughness values of Al_2O_3 coated PSS post treated with varying dosages of KF-99.

https://doi.org/10.61577/jcti.2024.100007

When the concentration of KF-99 reached 50% and 100%, the contact angles decreased to 142.5° and 108.5°, respectively. Surface roughness and chemical composition were identified as the reasons for hydrophobicity, with Al_2O_3-coated PSS having a roughness of 5.93 µm, compared to bare steel at 0.93 µm. This decreased to 3.09 µm with 10% KF-99 treatment and 3.78 µm with 20% KF-99 treatment. Higher concentrations of KF-99 (50% and 100%) resulted in a further decrease in roughness to 2.08 µm and 2.03 µm, respectively. The main reason for the enhanced water resistance of the coatings treated with 10% and 20% KF-99 was the presence of a rougher surface and the addition of methyl groups from silane units during treatment [27]. The silane moiety's dominance at higher concentrations (50% and 100%) led to a decrease in surface roughness influence, causing lower hydrophobicity than the 20% treatment [28]. Therefore, it was determined that a 20% KF-99 treatment was the most effective.

After heating the Al_2O_3-coated PSS with 20% KF-99 at 750°C, the water contact angle went down from 151.2° (cured sample) to 42.5°, just like the untreated Al_2O_3-coated PSS. Even with this decrease, the sintered coating still showed strong resistance to corrosion, as shown by E_{corr} and I_{corr} data (Table 2), resulting in a corrosion inhibition efficiency of 98.3%, demonstrating its exceptional anti-corrosion characteristics. The reason why hydrophobic and superhydrophobic properties occur after KF-99 treatment is due to the outward placement of hydrophobic methyl groups on the surface of the coating, which helps in water repellence and avoids contact with the metal surface. Figure 10(a) depicts the water repellent and corrosion resistant properties of the Al_2O_3-siloxane coating system. Improved resistance to corrosion in superhydrophobic coatings is due to the existence of air pockets in complex surface patterns, as shown in Figure 10(b) [12].

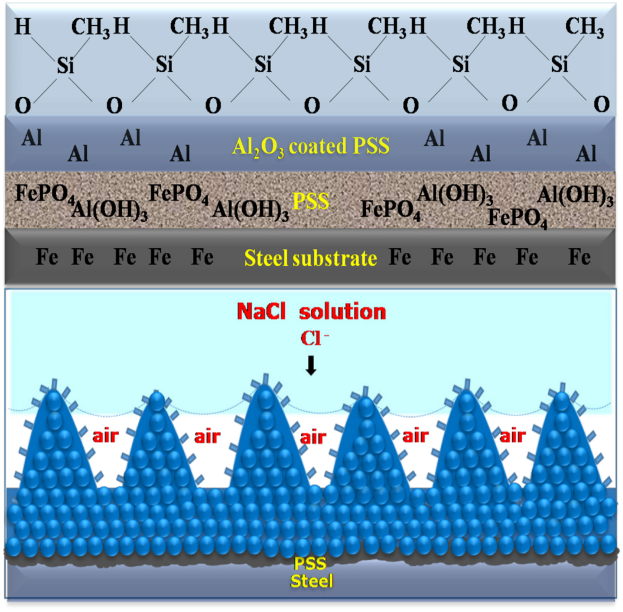

Figure 10. (a) Conceptual schematic diagram of the water repellency and corrosion resistance by Al_2O_3-siloxane coating system; (b) Model of the corrosion mechanism induced by superhydrophobic surface due to presence of air valley.

FTIR spectroscopic analysis

Analyzing the FTIR spectra of Al_2O_3-coated PSS and its treatment with different concentrations of KF-99 provides important information about how the coating system improves performance. At first, in the spectra of PSS coated with Al_2O_3, the distinct peaks at 1028 cm^-1, 1437 cm^-1, and 1643 cm^-1 are associated with stretching vibrations of PO, C=C, and COO bonds, respectively [22,29]. After being treated with KF-99, new peaks appear, suggesting that there are interactions between KF-99 and the Al_2O_3 coatings. Peaks at 932 cm^-1 represent stretching vibrations of Si-O-Al/Si-O-Fe, while 1070 cm^-1 and 1176 cm^-1 indicate linear and cross-linked Si-O-Si structures, respectively [24,30]. The modified chemical environment resulting from KF-99 treatment is highlighted by the presence of 1274 cm^-1 (Si-C) and 2170 cm^-1 (Si-H stretching) [31,32] (Figure 11).

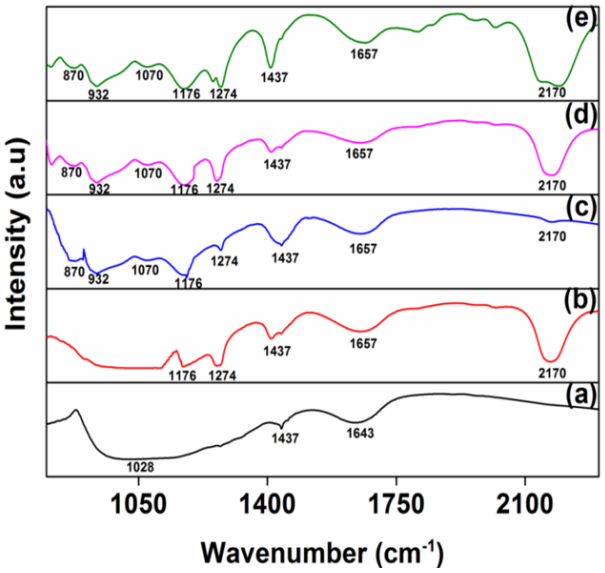

Figure 11. FTIR spectra of Al_2O_3 coated PSS (a), Al_2O_3 coated PSS post treated with 10 wt% (c), 20 wt% (d), 50 wt% (e), 100 wt% (f) KF-99, cured at 140°C for 2h.

The existence of Si-O-Al/Si-O-Fe bonds indicates enhanced adhesion of the coating to the steel base, essential for preventing corrosion. The Si-O-Si structure, with cross-links, improves the cohesion of the coating, creating a protective barrier against corrosive electrolytes and water from reaching the steel underneath [22]. This thorough FTIR analysis explains how KF-99 treatment changes the chemical bonds in Al_2O_3 coatings, improving their protective properties and longevity in harsh conditions.

Microstructural changes after electrochemical test

Figure 12 shows SEM pictures demonstrating the difference in corrosion resistance between mild steel surfaces with and without superhydrophobic coatings. Figure 12a shows the bare steel in its original condition, displaying a smooth, unbroken surface. After being in contact with a 3.5 wt% NaCl solution (Figure 12b), the steel without any protective coating shows visible cracks. On the other hand, Figure 12c shows the

https://doi.org/10.61577/jcti.2024.100007

superhydrophobic coating utilized with 20 wt% KF-99, showing a clean state before undergoing corrosion testing. Despite being exposed (Figure 12d), the coated substrate mostly stays intact. These results highlight the major improvement in protection against corrosion provided by the superhydrophobic coating, showcasing its promise in protective uses.

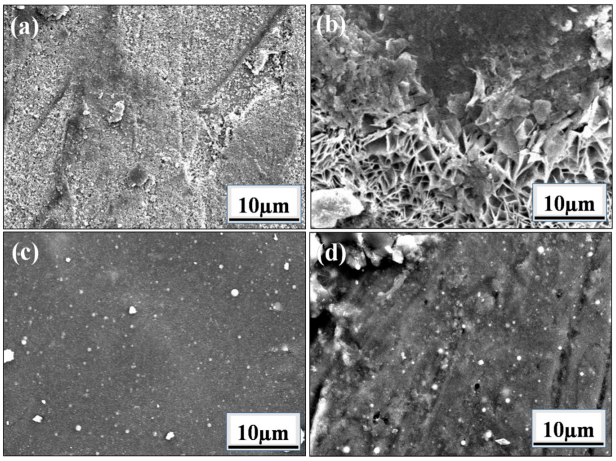

Figure 12. SEM images of bare steel before corrosion test (a), bare steel after corrosion test (b), superhydrophobic coating obtained with 20 wt% KF-99 before corrosion test (c), superhydrophobic coating obtained with 20 wt% KF-99 after corrosion test.

Conclusions

The need for high-quality, long-lasting, and eco-friendly coatings that shield materials from harsh environmental conditions is still crucial in today's industrial sectors. Nanostructured coatings that are superhydrophobic/hydrophobic present a potential answer to this issue, providing improved resistance to corrosion without harming the environment. This research investigates a new EPD method that utilizes ethanol as a suspension medium in order to create strong Al_2O_3-siloxane nanocomposite coatings. The coatings show excellent adhesion strength and outstanding corrosion resistance, along with superb superhydrophobic properties.

The EPD process outlined here is noteworthy for its ease, quickness, affordability, expandability, and eco-friendliness. Applying coatings through this technique shows impressive levels of corrosion inhibition: curing at 140°C results in 99.1% efficacy, while sintering at 750°C maintains a high efficiency of 98.3%. These coatings efficiently stop corrosive liquids from touching steel surfaces due to their extremely hydrophobic quality, forming "air valleys" in a rough surface structure, in addition to hydrophobic components. This characteristic makes them very appropriate for a variety of uses like pipelines, marine settings, cars, and aerospace parts.

The advancement of these coatings helps meet important industrial requirements by extending the longevity of materials in challenging environments, thus making a significant impact on the sustainability and effectiveness of multiple industries. Future research is focused on improving these coatings even more for wider commercial use, to ensure ongoing progress in protecting materials and the environment.

Acknowledgment

The authors are grateful to the Director, IMMT Bhubaneswar for permission to publish this paper. The contribution of Dr. Sarama Bhattacharjee, retired Chief Scientist for useful discussion and suggestion is greatly acknowledged.

Disclosure statement

No potential conflict of interest was reported by the authors.

References

1. Cost of corrosion, Global cost of corrosion. Nace study estimates global cost of corrosion at 25 trilliom Ann. NACE International. Accessed 08 March 2016. http://inspectioneering.com/news/2016-03-08/.
2. Bhaskaran R, Bhalla L, Rahman A, Juneja S, Sonik U, Kaur S, et al. An analysis of the updated cost of corrosion in India. Mater perform. 2014;53(8):56-65.
3. Döşlü ST, Mert BD, Yazıcı B. Polyindole top coat on TiO2 sol–gel films for corrosion protection of steel. Corros Sci. 2013;66:51-58. https://doi.org/10.1016/j.corsci.2012.08.067
4. Zheludkevich ML, Serra R, Montemor MF, Salvado IM, Ferreira MG. Corrosion protective properties of nanostructured sol–gel hybrid coatings to AA 2024-T3. Surf Coat Technol. 2006;200(9): 3084-3094. https://doi.org/10.1016/j.surfcoat.2004.09.007
5. Shen GX, Chen YC, Lin CJ. Corrosion protection of 316 L stainless steel by a TiO2 nanoparticle coating prepared by sol–gel method. Thin Solid Films. 2005;489(1-2):130-136. https://doi.org/10.1016/j.tsf.2005.05.016
6. Cecchetto L, Delabouglise D, Petit JP. On the mechanism of the anodic protection of aluminium alloy AA5182 by emeraldine base coatings: Evidences of a galvanic coupling. Electrochim Acta. 2007; 52(11):3485-3492. https://doi.org/10.1016/j.electacta.2006.10.009
7. Gray J, Luan B. Protective coatings on magnesium and its alloys—a critical review. J Alloys Compd. 2002;336(1-2):88-113. https://doi.org/10.1016/S0925-8388(01)01899-0
8. Singh Raman RK, Tiwari A. Graphene: The thinnest known coating for corrosion protection. Jom. 2014;66:637-642. https://doi.org/10.1007/s11837-014-0921-3
9. Guo SF, Zhang HJ, Liu Z, Chen W, Xie SF. Corrosion resistances of amorphous and crystalline Zr-based alloys in simulated seawater. Electrochem commun. 2012;24:39-42. https://doi.org/10.1016/j.elecom.2012.08.006
10. Wen YF, Cai CZ, Liu XH, Pei JF, Zhu XJ, Xiao TT. Corrosion rate prediction of 3C steel under different seawater environment by using support vector regression. Corros Sci. 2009;51(2):349-355. https://doi.org/10.1016/j.corsci.2008.10.038
11. Mohamed AM, Abdullah AM, Younan NA. Corrosion behavior of superhydrophobic surfaces: A review. Arb J Chem. 2015;8(6):749-765. https://doi.org/10.1016/j.arabjc.2014.03.006
12. Ishizaki T, Hieda J, Saito N, Saito N, Takai O. Corrosion resistance and chemical stability of super-hydrophobic film deposited on magnesium alloy AZ31 by microwave plasma-enhanced chemical vapor deposition. Electrochim Acta. 2010;55(23):7094-7101. https://doi.org/10.1016/j.electacta.2010.06.064
13. Chung JW, An BK, Kim JW, Kim JJ, Park SY. Self-assembled perpendicular growth of organic nanoneedles via simple vapor-phase deposition: one-step fabrication of a superhydrophobic surface. Chem commun. 2008(26):2998-3000. https://doi.org/10.1039/B802749H
14. Yu D, Tian J, Dai J, Wang X. Corrosion resistance of three-layer superhydrophobic composite coating on carbon steel in seawater. Electrochim Acta. 2013;97:409-419. https://doi.org/10.1016/j.electacta.2013.03.071
15. Qian B, Shen Z. Fabrication of superhydrophobic surfaces by dislocation-selective chemical etching on aluminum, copper, and zinc substrates. Langmuir. 2005;21(20):9007-9009.

https://doi.org/10.61577/jcti.2024.100007

https://doi.org/10.1021/la051308c
16. Khorsand S, Raeissi K, Ashrafizadeh F. Corrosion resistance and long-term durability of super-hydrophobic nickel film prepared by electrodeposition process. Appl Surf Sci. 2014;305:498-505. https://doi.org/10.1016/j.apsusc.2014.03.123
17. Sarkar P, Nicholson PS. Electrophoretic deposition (EPD): mechanisms, kinetics, and application to ceramics. J Am Ceram Soc. 1996;79(8):1987-2002. https://doi.org/10.1111/j.1151-2916.1996.tb08929.x
18. Besra L, Liu M. A review on fundamentals and applications of electrophoretic deposition (EPD). Prog Mater Sci. 2007;52(1):1-61. https://doi.org/10.1016/j.pmatsci.2006.07.001
19. Usha Kiran N, Dey S, Singh BP, Besra L. Graphene coating on copper by electrophoretic deposition for corrosion prevention. Coatings. 2017;7(12):214. https://doi.org/10.3390/coatings7120214
20. Singh BP, Nayak S, Nanda KK, Jena BK, Bhattacharjee S, Besra L. The production of a corrosion resistant graphene reinforced composite coating on copper by electrophoretic deposition. Carbon. 2013;61:47-56. https://doi.org/10.1016/j.carbon.2013.04.063
21. Zhan-Fang C, Pei Q, Pei C, Xin W, Guang-Yi L, Shuai W, et al. Super-hydrophobic coating used in corrosion protection of metal material: review, discussion and prospects. Metall Res Technol. 2017;114(2):203. https://doi.org/10.1051/metal/2017011
22. Dey S, Chatterjee S, Singh BP, Bhattacharjee S, Rout TK, Sengupta DK, et al. Development of superhydrophobic corrosion resistance coating on mild steel by electrophoretic deposition. Surf Coat Technol. 2018;341:24-30. https://doi.org/10.1016/j.surfcoat.2018.01.005
23. Popić JP, Jegdić BV, Bajat JB, Mitrić M, Mišković-Stanković VB. Surface coverage determination of iron-phosphate coatings on steel using voltammetric anodic dissolution technique. J Serb Chem Soc. 2013;78(1):101-114. https://doi.org/10.2298/JSC120706096P
24. Yang L, Zhang W, Gu T, Feng J. Influence of acetic acid on dynamic behavior of hydrolazation and film forming of organosilane. J Wuhan Univ Technol-Mater. Sci Ed. 2009;24(4):546-551. https://doi.org/10.1007/s11595-009-4546-2
25. Musil J, Jirout M. Toughness of hard nanostructured ceramic thin films. Surf Coat Technol. 2007;201(9-11):5148-5152. https://doi.org/10.1016/j.surfcoat.2006.07.020
26. Vazirinasab E, Jafari R, Momen G. Application of superhydrophobic coatings as a corrosion barrier: A review. Surf Coat Technol. 2018;341:40-56. https://doi.org/10.1016/j.surfcoat.2017.11.053
27. Wang Y, Wang P, Kohls D, Hamilton WA, Schaefer DW. Water absorption and transport in bis-silane films. Phys Chem Chem Phys. 2009;11(1):161-166. https://doi.org/10.1039/B808741E
28. Kumar D, Wu X, Fu Q, Ho JW, Kanhere PD, Li L, et al. Hydrophobic sol–gel coatings based on polydimethylsiloxane for self-cleaning applications. Mater Des. 2015;86:855-862. https://doi.org/10.1016/j.matdes.2015.07.174
29. Yagyu S, Yoshitake M, Tsud N, Chikyow T. Adsorption structure of phenylphosphonic acid on an alumina surface. Appl Surf Sci. 2009; 256(4):1140-1143. https://doi.org/10.1016/j.apsusc.2009.05.110
30. Kunst SR, Cardoso HR, Oliveira CT, da Silva Filho CI, Sarmento VH, Menezes TL, et al. Influence of tetraethoxysilane addition in siloxane-poly (methyl methacrylate) hybrid films applied on galvanized steel. Int J Electrochem Sci. 2013;8(10):11984-2004. https://doi.org/10.1016/S1452-3981(23)13237-8
31. Parale VG, Mahadik DB, Phadtare VD, Pisal AA, Park HH, Wategaonkar SB. Dip coated superhydrophobic and anticorrosive silica coatings. Int J Mater Sci Eng. 2016;4(1):60-67. https://doi.org/10.17706/ijmse.2016.4.1.60-68
32. Lucovsky G, Nemanich RJ, Knights JC. Structural interpretation of the vibrational spectra of a-Si: H alloys. Phys Rev B. 1979;19(4):2064. https://doi.org/10.1103/PhysRevB.19.2064

https://doi.org/10.61577/jcti.2024.100007